https://dx.doi.org/10.21577/0103-5053.20210145

J. Braz. Chem. Soc., Vol. 33, No. 3, 268-273, 2022
©2022 Sociedade Brasileira de Química

Article

Structural Characteristics of Lignite Char from Different Pyrolysis Reactors and the Influence on Their Gasification Reactivity

Ying Zhang, *,[a] *Haitang Wang*[a] *and Xiaoqin Wang*[a]

[a]*Shanxi Institute of Energy, 030600 Jinzhong, China*

The gasification reactivity of coal char is affected by numerous experimental variables, and char structure is one of the dominant factors. In this work, Raman spectroscopy, powder X-ray diffraction (XRD), and N_2 adsorption were used to investigate the physical and chemical structure of char prepared under different pyrolysis conditions. Three kinds of pyrolysis reactors, fluidized-bed reactor (FL), entrained-flow-bed reactor (EF), and fixed-bed reactor (PT), were designed and used to prepare the char samples. Lignite was pyrolyzed in a fixed-bed reactor with a heating rate of 10 ºC min^{-1}, and the final temperature was 1000 ºC. The gasification reactivity of char was characterized in a quartz fixed-bed reactor under CO_2, H_2O, and their mixtures at 750 ºC. FB reactor produces chars with a smaller interlayer spacing of aromatic layers (d_{002}), and FL reactor produces chars with a larger mean crystallite size along the c-axis (L_c) and aromaticity (f_a) but inhibits the growth of mean crystallite size along the a-axis (L_a). The content of small aromatic rings, which is higher in the FL reactor, positively affects the initial intrinsic reactivity.

Keywords: pyrolysis reactors, char gasification, structural evolution, gasification reactivity

Introduction

Coal continues to be an essential energy source in many parts of the world, especially in China and Australia. Developing and utilizing coal resources rationally, efficiently, and environmentally is a reasonable way to alleviate the pressure of energy demand. Thus, a deeper understanding of coal structure and property becomes more important for the development of clean coal utilization.[1,2] The organic structure of coal can be regarded as heterogeneous aromatic compounds, with increasing aromaticity from low rank to high rank coals.[3-5] As a low rank coal, lignite is a cheap fuel and is usually low in sulfur. On account of the over-exploitation of hard coal, more and more attention has been drawn to the exploration and utilization of lignite. The existing lignite reserves in China are about 129 billion tons, accounting for 12.9% of the total Chinese coal reserves. However, high moisture content (25-50%) in lignite causes serious application problems, and it is generally difficult to be ground, separated, and classified. Approaches such as drying and pyrolysis are often used to upgrade lignite before the subsequent utilization process.[6-8] Nowadays, gasification has been an efficient thermal conversion process to upgrade lignite. The gasification of coal char with low-quality lignite as raw material expands the utilization range of inferior coal. It generates synthetic gas as the main product, which invigorates the downstream capacity of the char industry chain.[9-12] In the actual industrial production process, the characteristics of coal species and the difference of process conditions will cause significant changes to the char structure and further affect the gasification efficiency. At present, studies on the correlation between chemical structure and gasification characterization of coal char, especially between coal char and gasification under H_2O and CO_2, are still lacking. The development and utilization of existing equipment remain an expensive and time-consuming process, and the data provided can only be applied to a specific process.[10,13-15] Therefore, it is of great significance to research coal char reactivity through the correlation between coal char structure and gasification reactivity, and finally realize the purpose of predicting the gasification reactivity of coal char based on the natural property of raw coal.

Many advanced techniques have been used to characterize the chemical and physical structures of coal char, such as Fourier transform infrared spectroscopy (FTIR), Raman spectroscopy, X-ray diffraction (XRD), N_2 adsorption, and scanning electron microscope (SEM). Also, XRD has been commonly used to investigate the crystalline structure of coal char, among which some features are

*e-mail: zysxnyxy@163.com
Editor handled this article: Jaísa Fernandes Soares

Table 1. Proximate and ultimate analysis of lignite char

Sample	Proximate analysis / wt.%				Ultimate analysis / wt.%			
	M_{ad}	A_d	V_{daf}	C_{daf}	H_{daf}	O^a	N_{daf}	S_d
L-1000PT	3.29	13.62	3.47	96.79	0.55	1.12	1.14	0.33
L-1000FL	2.21	11.90	5.84	92.62	1.36	4.61	1.04	0.30
L-1000EF	4.18	14.45	7.31	93.77	1.50	3.11	1.16	0.29

[a]By difference. M: moisture content; A: ash content; V: volatile matter; subscript ad: air dried basis; d: dry basis; daf: dry and ash free basis.

related to gasification or combustion reactivity.[16,17] It has been reported that char crystallinity and highly ordered carbonaceous material negatively correlate with gasification and combustion reactivity.[18,19]

Some researchers used Raman spectroscopy to characterize the structural features of carbonaceous materials, including coals and chars, and D band (reflecting the disordered structure in graphite or other highly ordered carbonaceous materials) and G band (graphite E^2_{2g} band) were usually assigned.[5,20-26] While these two bands cannot make an accurate structural description, since there are many overlapped peaks between the D band and G band, which contain some rich information about the actual structural feature of lignite char. A series of studies on the structure of coal or coal char using Raman technique has been conducted by Li *et al.*[24-26] and the Raman spectra are generally deconvoluted into 10 bands to acquire detailed information about the skeletal structure of lignite char.

The gasification of coal char with H_2O is a fundamental reaction in a gasifier, and CO_2, which also acts as a kind of gasification agent, is one of the components in flue gas and can partially replace H_2O. However, the relationship between intrinsic gasification reactivity and the structural feature of lignite char in these atmospheres remains unclear. Thus, this work aims to study the structural feature of lignite char from three different reactors, fixed-bed reactor (PT), fluidized-bed reactor (FL), and entrained-flow-bed reactor (EF), and investigate the influence on their gasification reactivity in H_2O and CO_2.

Experimental

Sample preparation

A Chinese lignite was used in this study, and the sample was pulverized and sieved to 96-150 μm. In this study, coal samples were prepared in three different pyrolysis reactors with a final pyrolysis temperature of 1000 ºC. 10 g sample was put into the fixed-bed reactor and heated at 10 ºC min^{-1} under N_2, the flow rate of N_2 was 600 mL min^{-1} (L-1000PT). In FL and EF, the sample is heated from 25 to 1000 ºC and the sampling rate was 0.2 g min^{-1}, then held at 1000 ºC for 1 h with a N_2 flow rate of 5000 mL min^{-1} in FL (L-1000FL) and 600 mL min^{-1} in EF (L-1000EF), respectively. After that, the samples in the collection bottle are cooled to room temperature under N_2. The proximate and ultimate analyses of produced lignite chars (L-1000PT, L-1000FL, L-1000EF) are listed in Table 1.

Char characterization

Raman spectra of chars were recorded with a Renishaw inVia Raman spectrometer (New Mills, United Kingdom). The excitation Nd:YAG laser wavelength was 541.5 nm; the laser power was 20 mW. The recorded Raman spectra in the range between 800 and 1800 cm^{-1} were curve-fitted using Origin software[27] with 10 Gaussian bands. One example of spectral deconvolution is given in Figure 1 (the detailed methodology of band assignment has been reported in references 24-26).

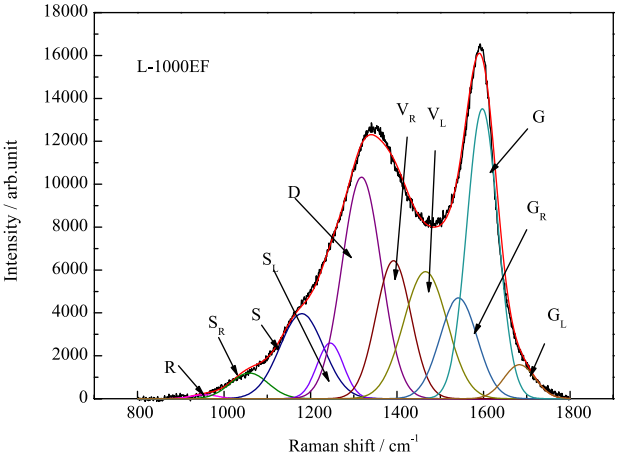

Figure 1. Curve fitting of the Raman spectrum of L-1000EF.

The carbon microcrystalline structure was characterized by the Miniflex II X-ray diffraction (XRD) instrument (Tokyo, Japan), using the Kα radiation of Cu. The scanning range (2θ) was from 10º to 80º with a step size of 0.01º. Operating conditions were: tube voltage 40 kV, tube current 100 mA, graphite monochrome filter. Under this condition, the data of carbon microcrystalline structure was obtained

by scanning the diffraction peak position and diffraction peak strength of the measured spectrum.

In the experiment, the low-temperature nitrogen adsorption method was used. The high purity N_2 of the test gas was −196 ºC, the pressure point interval was 0.1 KPa. The pore structure and surface area of the char samples were calculated using Barrett-Joyner-Halenda (BJH) and Brunauer-Emmett-Teller (BET) method.

Reactivity measurements

Reactivity measurements were conducted in a laboratory-scale fixed-bed quartz reactor at 1000 ºC. The reactor suspends approximately 1.5 g of char on a quartz frit, into which a thermocouple is inserted to measure the temperature of the sample bed. Reactant gas (30% H_2O + 30% CO_2 + 40% N_2) was passed through the entire sample, and measurements of gas concentration and flow rates were used to determine reaction rates.

The carbon conversion (x) is calculated by equation 1:

$$x = \frac{w_0 - w}{w_0} \quad (1)$$

where w_0 and w represent the initial weight (daf) and the weight (daf) of char at reaction time t, respectively.

The specific reaction rate (r) is the as-measured reaction rate and calculated with the expression in equation 2:

$$r = -\frac{1}{w}\frac{dw}{dt}\left(g\ g^{-1}\ s^{-1}\right) \quad (2)$$

The intrinsic reaction rate (r_{int}) is the reaction rate that eliminates the effect of specific surface area and calculated by equation 3:

$$r_{int} = \frac{r}{S} \quad (3)$$

where S represents the specific surface area of char.

Results and Discussion

XRD analysis

Figure 2 shows the XRD diagram of chars pyrolyzed in FL, EF, and PT reactors at 1000 ºC. It can be seen that the 002 peak of L-1000FL is much thinner and higher than that of L-1000EF and L-1000PT, and the 002 peak position of L-1000FL is moved to a higher degree, which indicates a better crystalline structure and a higher content of aromatic carbon. At the same time, the 100 peak of the L-1000FL is also narrower than those obtained from the other two reactors, indicating that the average size of the aromatic wafer layer in L-1000FL is relatively smaller.

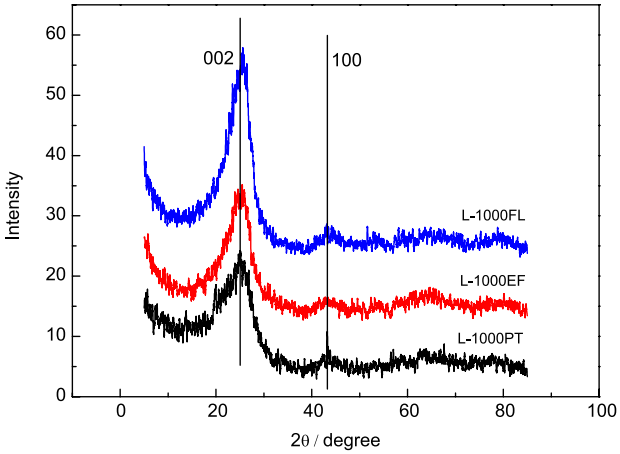

Figure 2. XRD diagram of chars from different reactors at 1000 ºC.

To analyze the XRD diagram quantitatively, the 002 peak should be curve fitted. One assumption should be treated as a premise that the 002 peak and γ peak were symmetrical peaks, and the peak position of γ peak is far away from 002 peak without any effect on its right.[16,17] An example of XRD spectral deconvolution is given in Figure 3.

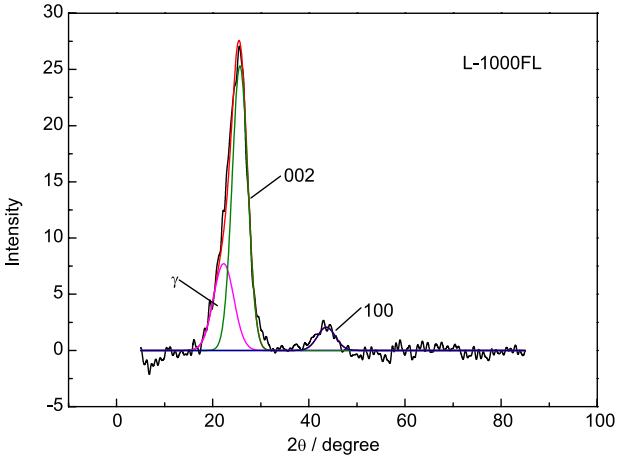

Figure 3. Curve fitting of XRD spectra of L-1000FL.

After curve fitting and calculating, the relevant data are shown in Table 2. The microcrystalline structural parameters of chars from different pyrolysis reactors are also various. The interlayer spacing of aromatic layers (d_{002}) of L-1000FL and L-1000PT seems less than L-1000EF. This could be attributed to that a longer holding time in the pyrolysis reactor contributes to a denser microcrystalline structure for lignite char. However, L-1000FL has the maximum L_c

(crystallite height) and f_a (aromaticity) value but minimum L_a (crystallite diameter) value. The interactions between volatile matters and chars may positively affect the growth of mean crystallite size along the c-axis and a reverse effect on that along the a-axis.

Table 2. Microcrystalline structural parameters of chars from different reactors at 1000 ℃

Sample	d_{002} / nm	L_c / nm	L_a / nm	f_a
L-1000FL	0.32	1.789	0.891	0.716
L-1000EF	0.373	1.790	1.199	0.694
L-1000PT	0.310	1.780	1.154	0.663

d_{002}: interlayer spacing; L_c: crystallite height; L_a: crystallite diameter; f_a: aromaticity; FL: fluidized-bed reactor; EF: entrained-flow-bed reactor; PT: fixed-bed reactor.

Pore structure and specific surface area analysis

Previous works[11,14] have studied the effects of different atmospheres and pressure on pore structure and specific surface area. Still, the research for the impact of reactors on pore structure and specific surface area is not sufficient. Figures 4 and 5 show the pore structure and specific surface area of chars from different pyrolysis reactors.

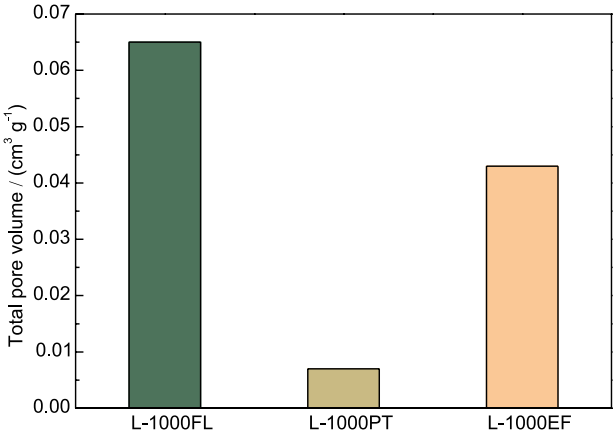

Figure 4. Effect of pyrolysis reactors on total pore volume.

The total pore volume and specific surface area of chars in FL and EF are much higher than in PT. At the same final temperature and holding time, devolatilization in FL is much more severe, and drastic devolatilization may lead to a richer pore structure and a larger specific surface area.[28] The heating rate has a significant impact on the expansivity of samples, and a higher heating rate will increase the expansivity of chars.[29] The heating rate in EF is much higher than that in PT which is only 10 ℃ min^{-1}, so the expansion behavior in L-1000EF is much more drastic than L-1000PT, resulting in a higher total pore volume and specific surface area.

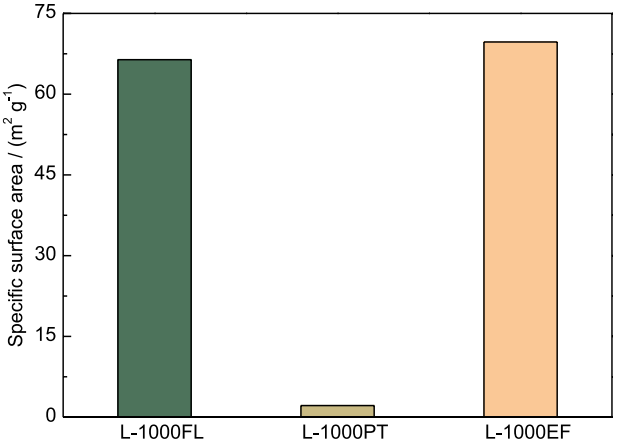

Figure 5. Effect of pyrolysis reactors on the specific surface area.

Raman spectra analysis

Raman spectra of samples were obtained to investigate the relationship between the char chemical structure and intrinsic reactivity. The spectra were deconvoluted in 10 Gaussian bands. Previous works[12,24,26] show that four main factors will affect the total Raman intensity: the concentration of samples, the Raman scattering ability, the light absorptivity, and the presence of electron-rich functional groups. Figure 6 gives the result that seems to be related to the variations in the amount of electron-rich groups in different reactors. The difference of electron-rich O-containing functional groups shown in Table 1 may lead to the variation of total Raman intensity of samples.

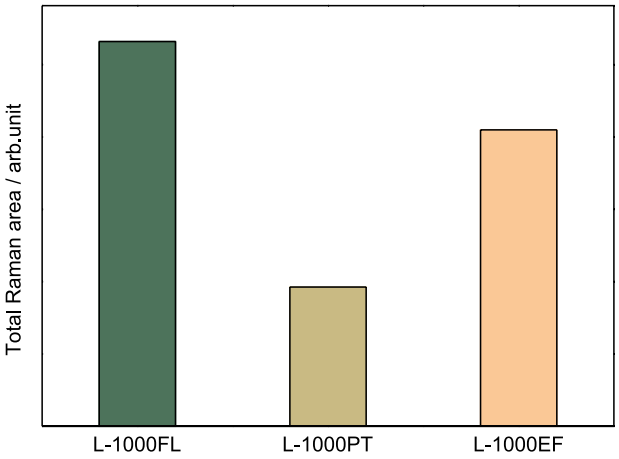

Figure 6. Raman peak areas of chars pyrolized in different reactors at 1000 ℃.

Figure 7 shows the band ratios of chars from different pyrolysis reactors. The ratio of the intensity of D band (I_D) and the intensity of G band (I_G) is treated as an essential index to investigate the crystal and graphite-like carbon structure. The decrease of I_D/I_G ratio normally presences

an increasing extent of graphitization. The S band mainly represents sp^3-rich structures such as alkyl-aryl C–C structures and methyl carbon dangling to an aromatic ring. In particular, the S band can be considered as a brief measure of cross-linking density and substitutional groups. The ratio $I_D/I_{(Gr + Vr + Vl)}$ can be taken as a brief measure of the ratio between the large aromatic ring systems (≥ 6 rings) and the aromatic ring systems typically found in amorphous carbon. In Figure 7, the ratio I_D/I_G gives the information that the content of ordered structure in chars from PT reactor is higher than that from FL and EF reactors, indicating that the pyrolysis condition in PT reactor is more beneficial for graphitization of chars. The ratio I_S/I_G indicates that pyrolysis conditions in EF and FL reactors produce more drastic chars' cross-linking behavior than in the PT reactor. The ratio $I_D/I_{(Gr + Vr + Vl)}$ shows that a relatively moderate heating process and interaction of volatile matter in PT reactor promote the conversion of small aromatic rings (< 6 rings) structures to large aromatic rings (≥ 6 rings) structures than that in EF and FL reactors.

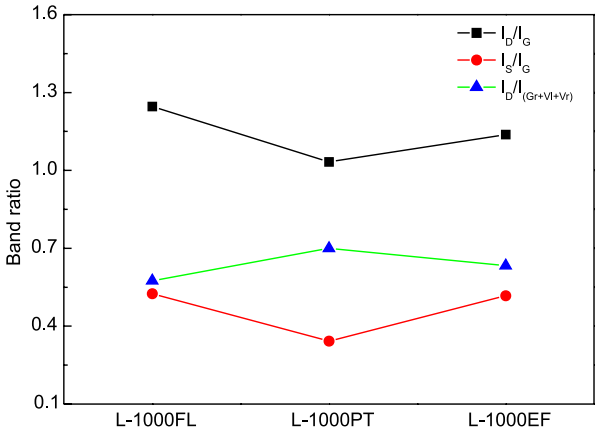

Figure 7. Band ratios as a function of chars from different reactors at 1000 ºC.

Char reactivity

The intrinsic reactivity could eliminate the surface area effects associated with the specific rate and reflect the inherent features of the char surface and the influence of mineral matter and other impurities. Figure 8 shows the intrinsic reaction rate as a function of carbon conversion during reaction with CO_2, steam, and their mixture at 750 ºC. Figure 8 indicates that the intrinsic reactivity in mixture agents is lower than that in steam but higher than that in CO_2, demonstrating an interaction between C–CO_2 and C–H_2O reactions, but the mechanism is unclear.

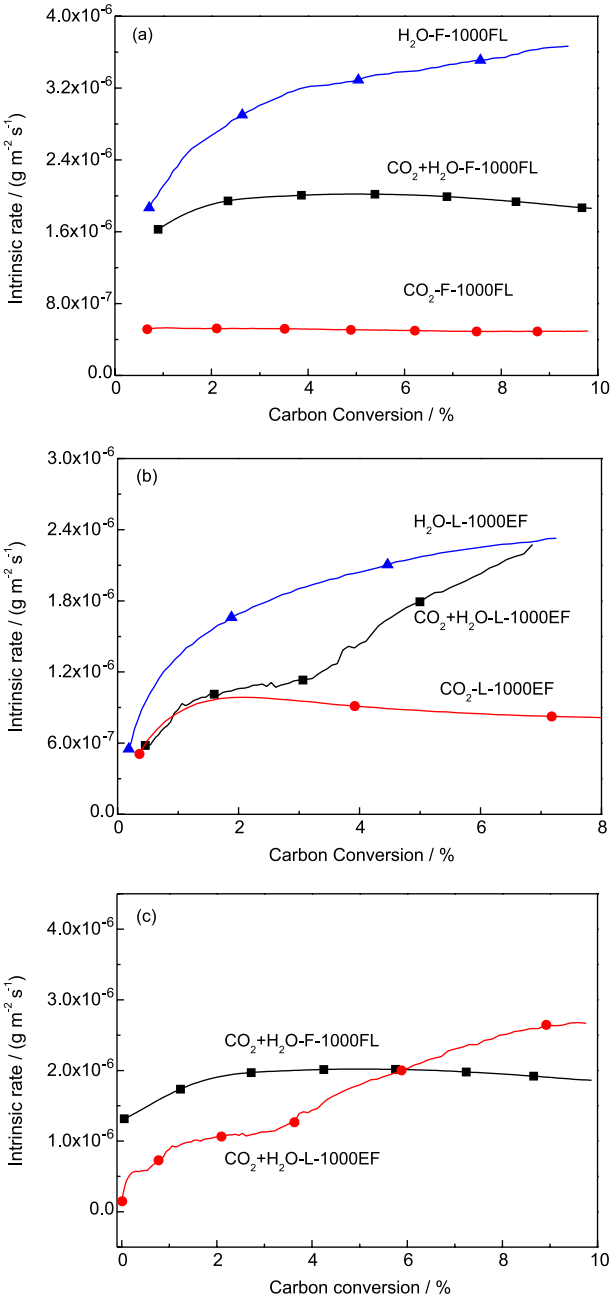

Figure 8. Comparison of the intrinsic rate of chars from FL and EF reactors with different gasification agents.

Relationships between the structure and intrinsic reactivity

The intrinsic reactivity of co-gasification has a good relationship with the structure of lignite char. The value $I_D/I_{(Gr + Vr + Vl)}$ of L-1000FL is lower than that of L-1000EF, which reveals that there are more small aromatic rings structures in chars from FL reactor than those from EF reactor, and this difference reflects a higher initial intrinsic reactivity (conversion less than 5%) of chars in FL reactor than that in EF reactor. After 5% conversion, the intrinsic reactivity of L-1000EF exceeds that of L-1000FL, which

may be caused by the changes of the content of small aromatic rings structure, but it is not clear in this research.

Conclusions

The physical and chemical structures of char samples, and intrinsic rates of lignite char gasification in CO_2, H_2O and their mixtures, were studied. Total pore volume and specific surface area were used to characterize the physical structure of chars. XRD and Raman features were used to characterize the chemical structure of chars and part of them were used to interpret relative coal char reactivity.

Pyrolysis in PT reactor produces a char with smaller interlayer spacing of aromatic layers (d_{002}). FL reactor produces a char with larger mean crystallite size along the c-axis (L_c) and aromaticity (f_a), but inhibit the growth of mean crystallite size along the a-axis (L_a). More drastic devolatilization in FL reactor produces a char that is rich in pore volume.

The intrinsic reactivity of gasification with mixtures of CO_2 and steam is lower than that under steam atmosphere but higher than in CO_2. The content of small aromatic rings affects the initial intrinsic reactivity, but with the conversion of chars, the change rate of small aromatic rings content may vary from chars in different pyrolysis reactors. This suggests that a study on structural changes of chars from different pyrolysis reactors *versus* carbon conversion is necessary, which will help get more details about the effects of reactors on char structures.

Acknowledgments

The authors gratefully acknowledge the financial support from the Shanxi Institute of Energy Project (ZY-2017005).

References

1. Chen, X.; Zheng, D.; Guo, J.; Liu, J.; Ji, P.; *Energy* **2013**, *52*, 279.
2. Baysal, M.; Yürüm, A.; Yıldız, B.; Yürüm, Y.; *Int. J. Coal Geol.* **2016**, *163*, 166.
3. Oikonomopoulos, I. K.; Perraki, M.; Tougiannidis, N.; Perraki, T.; Frey, M. J.; Antoniadis, P.; Ricken, W.; *Int. J. Coal Geol.* **2013**, *115*, 1.
4. He, X.; Liu, X.; Nie, B.; Song, D.; *Fuel* **2017**, *206*, 555.
5. Ulyanova, E. V.; Molchanov, A. N.; Prokhorov, I. Y.; Grinyov, V. G.; *Int. J. Coal Geol.* **2014**, *121*, 37.
6. Tahmasebi, A.; Yu, J.; Han, Y.; Li, X.; *Fuel Process. Technol.* **2012**, *101*, 85.
7. Zhao, H.; Song, Q.; Liu, S.; Li, Y.; Wang, X.; Shu, X.; *Energy Convers. Manage.* **2018**, *161*, 13.
8. Zhao, H.; Li, Y.; Song, Q.; Liu, S.; Ma, L.; Shu, X.; *Fuel* **2021**, *286*, 119398.
9. Roberts, D. G.; Harris, D. J.; *Fuel* **2007**, *86*, 2672.
10. Jing, X.; Wang, Z.; Zhang, Q.; Yu, Z.; Li, C.; Huang, J.; Fang, Y.; *Energy Fuels* **2013**, *27*, 7287.
11. Tay, H. L.; Kajitani, S.; Zhang, S.; Li, C. Z.; *Fuel* **2013**, *103*, 22.
12. Wang, M.; Shen, Y.; Guo, P.; Kong, J.; Wu, Y.; Chang, L.; Wang, J.; Xie, W.; *J. Anal. Appl. Pyrolysis* **2020**, *149*, 104859.
13. Yu, J.; Guo, Q.; Ding, L.; Gong, Y.; Yu, G.; *Fuel* **2020**, *270*, 117603.
14. Wang, D.; Yang, H.; Wu, Y.; Zhao, C.; Ju, F.; Wang, X.; Zhang, S.; Chen, H.; *J. Energy Inst.* **2020**, *93*, 1999.
15. Liu, X.; Zheng, Y.; Liu, Z.; Ding, H.; Huang, X.; Zheng, C.; *Fuel* **2015**, *157*, 97.
16. Wu, S.; Gu, J.; Zhang, X.; Wu, Y.; Gao, J.; *Energy Fuels* **2008**, *22*, 199.
17. Everson, R. C.; Okolo, G. N.; Neomagus, H. W. J. P.; dos Santos, J. M.; *Fuel* **2013**, *109*, 148.
18. Sonibare, O. O.; Haeger, T.; Foley, S. F.; *Energy* **2010**, *35*, 5347.
19. Liu, M.; Bai, J.; Yu, J.; Kong, L.; Bai, Z.; Li, H.; He, C.; Ge, Z.; Cao, X.; Li, W.; *Energy Fuels* **2020**, *34*, 4162.
20. Guedes, A.; Valentim, B.; Prieto, A. C.; Noronha, F.; *Fuel* **2012**, *97*, 443.
21. Hinrichs, R.; Brown, M. T.; Vasconcellos, M. A. Z.; Abrashev, M. V.; Kalkreuth, W.; *Int. J. Coal Geol.* **2014**, *136*, 52.
22. Li, K.; Khanna, R.; Zhang, J.; Barati, M.; Liu, Z.; Xu, T.; Yang, T.; Sahajwalla, V.; *Energy Fuels* **2015**, *29*, 7178.
23. Okolo, G. N.; Neomagus, H. W. J. P.; Everson, R. C.; Roberts, M. J.; Bunt, J. R.; Sakurovs, R.; Mathews, J. P.; *Fuel* **2015**, *158*, 779.
24. Li, X.; Hayashi, J.-i.; Li, C. Z.; *Fuel* **2006**, *85*, 1700.
25. Zhang, S.; Min, Z.; Tay, H. L.; Asadullah, M.; Li, C. Z.; *Fuel* **2011**, *90*, 1529.
26. Li, T.; Zhang, L.; Dong, L.; Li, C. Z.; *Fuel* **2014**, *117*, 1190.
27. *Origin*, 2018b; OriginLab, Northampton, USA, 2018.
28. Li, S. F.; Wu, S. Y.; *J. Fuel Chem. Technol.* **2010**, *38*, 513.
29. Zhang, H.; Pu, W. X.; Ha, S.; Li, Y.; Sun, M.; *Fuel* **2009**, *88*, 2303.

Submitted: August 9, 2021
Published online: October 27, 2021

This is an open-access article distributed under the terms of the Creative Commons Attribution License.